



Neutron powder diffraction study of the magnetic and crystal structures of $\text{SrFe}_2(\text{PO}_4)_2$

Alexei A. Belik^{a,*}, Qingzhen Huang^b, Eiji Takayama-Muromachi^a, Jeffrey W. Lynn^b

^a International Center for Materials Nanoarchitectonics (MANA), National Institute for Materials Science (NIMS), 1-1 Namiki, Tsukuba, Ibaraki 305-0044, Japan

^b NIST Center for Neutron Research, National Institute of Standards and Technology, Gaithersburg, MD 20899, USA

ARTICLE INFO

Article history:

Received 22 January 2008

Received in revised form

12 May 2008

Accepted 17 May 2008

Available online 28 May 2008

Keywords:

Neutron powder diffraction

Magnetic structure

Crystal structure

Low-dimensional magnets

ABSTRACT

The crystal and magnetic structures of $\text{SrFe}_2^+(\text{PO}_4)_2$ have been determined by neutron powder diffraction data at low temperatures (space group $P2_1/c$ (no. 14); $Z = 4$; $a = 9.35417(13)\text{Å}$, $b = 6.83808(10)\text{Å}$, $c = 10.51899(15)\text{Å}$, and $\beta = 109.5147(7)^\circ$ at 15 K). Two magnetic phase transitions were found at $T_1 = 7.4\text{ K}$ (first-order phase transition) and $T_2 = 11.4\text{ K}$ (second-order phase transition). The transition at T_2 was hardly detectable by dc and ac magnetization measurements, and a small anomaly was observed by specific heat measurements. At T_1 , strong anomalies were found by dc and ac magnetization and specific heat. The structure of $\text{SrFe}_2(\text{PO}_4)_2$ consists of linear four-spin cluster units, Fe2-Fe1-Fe1-Fe2 . Below T_1 , the propagation vector of the magnetic structure is $k = [0,0,0]$. The magnetic moments of the inner Fe1-Fe1 atoms of the four-spin cluster unit are ferromagnetically coupled. The magnetic moment of the outer Fe2 atom is also ferromagnetically coupled with that of the Fe1 atom but with spin canting. The four-spin cluster units form ferromagnetic layers parallel to the $[-101]$ plane, while these layers are stacked antiferromagnetically in the $[-101]$ direction. Spin canting of the outer Fe2 atoms provides a weak ferromagnetic moment of about $1\mu_B$ along the b -axis. The refined magnetic moments at 3.5 K are $4.09\mu_B$ for Fe1 and $4.07\mu_B$ for Fe2 . Between T_1 and T_2 , a few weak magnetic reflections were observed probably due to incommensurate magnetic order.

© 2008 Elsevier Inc. All rights reserved.

1. Introduction

Magnetic properties including magnetic structures of low-dimensional and frustrated magnets have attracted much attention in recent years in part because of the great interest in multiferroic materials [1,2]. In multiferroic materials, magnetism and (anti)ferroelectricity coexist [3]. Usually the coupling between different order parameters is weak in multiferroics. However it was found that dielectric properties can strongly depend on applied magnetic fields if ferroelectricity is caused by specific magnetic ordering (e.g., spiral and helical magnetic ordering with appropriate crystal symmetry). Recent discoveries showed that a number of well-known low-dimensional compounds such as MnWO_4 [4], LiCu_2O_2 [5], LiCuVO_4 [6], $\text{Ni}_3(\text{VO}_4)_2$ [7], and pyroxenes [8] possess multiferroic properties. Therefore, investigation of magnetic structures of low-dimensional magnets is essential work in searching for new multiferroics.

Phosphates containing transition metals have been widely investigated because complex structural chemistry of phosphates offers large variations of magnetic ion sublattices, which can give

rise to original magnetic properties. Magnetic structures of simple (e.g., FePO_4 [9], CrPO_4 [10], and $\text{Ni}_3(\text{PO}_4)_2$ [11]) and more complex phosphates (e.g., $\text{CuNi}_2(\text{PO}_4)_2$ [12] and $\text{Co}_2(\text{OH})\text{PO}_4$ [13]) have been reported. Compounds with the nominal composition of $A^{2+}B_2^+(\text{PO}_4)_2$ ($A = \text{Ca}, \text{Sr}, \text{Ba}, \text{and Pb}$; $B = \text{Mg}$ and divalent transition metals) show large variations in crystal structures. About ten structure types are known for this family that includes $\text{CaCr}_2(\text{PO}_4)_2$ [14], $\text{SrMn}_2(\text{PO}_4)_2$ [15], $\text{SrCo}_2(\text{PO}_4)_2$ [16], $\text{SrNi}_2(\text{PO}_4)_2$ [17], $\alpha\text{-SrZn}_2(\text{PO}_4)_2$ [18], $\text{BaCo}_2(\text{PO}_4)_2$ [19], $\text{BaCu}_2(\text{PO}_4)_2$ [20], $\text{SrMg}_2(\text{PO}_4)_2$ [21], $\beta\text{-SrZn}_2(\text{PO}_4)_2$ [21], $\text{SrCd}_2(\text{PO}_4)_2$ [22], $\text{BaNi}_2(\text{PO}_4)_2$ [23], $\text{SrCu}_2(\text{PO}_4)_2$ [24], and $\text{PbCu}_2(\text{PO}_4)_2$ [25,26]. $\text{BaNi}_2(\text{PO}_4)_2$ was considered as a model of a two-dimensional XY antiferromagnet. $\text{SrCu}_2(\text{PO}_4)_2$ and $\text{PbCu}_2(\text{PO}_4)_2$ showed spin-gap behavior due to the presence of linear four-spin clusters. $\text{BaCu}_2(\text{PO}_4)_2$ also showed spin-gap behavior, but the magnetic lattice was not well understood.

The crystal structure of another member of the $AB_2(\text{PO}_4)_2$ family, $\text{SrFe}_2(\text{PO}_4)_2$ [27], has recently been determined at room temperature (RT) from X-ray powder diffraction data [28]. It comprises almost linear four-ion clusters (Fig. 1) that are arranged in two-dimensional layers along the c -axis (Fig. 2a). Two phase transitions were found in $\text{SrFe}_2(\text{PO}_4)_2$ at low temperatures at $T_1 = 7.0$ and $T_2 = 11.3\text{ K}$ by specific heat measurements [28]. The phase transition at T_2 was supposed to be a structural phase

* Corresponding author. Fax: +81 29 860 4706.

E-mail address: Alexei.BELIK@nims.go.jp (A.A. Belik).

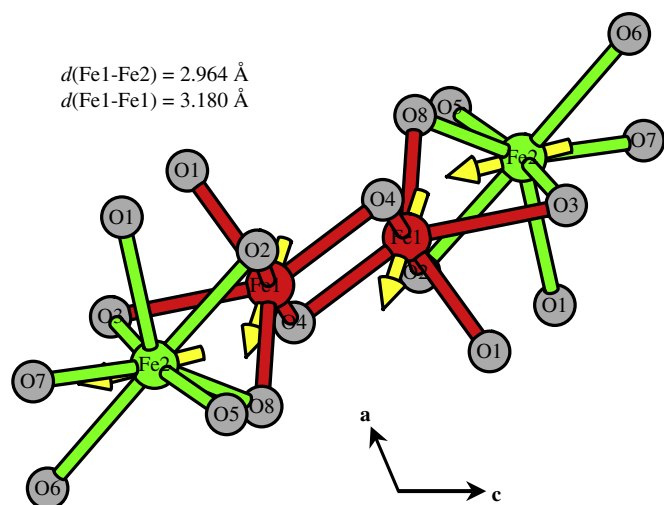


Fig. 1. Four-spin cluster unit (Fe_4O_{18}) in $\text{SrFe}_2(\text{PO}_4)_2$ [28]. The arrows on the Fe atoms show the direction of magnetic moments at 3.5 K determined in this work. Fe–Fe distances in the four-spin cluster unit are given.

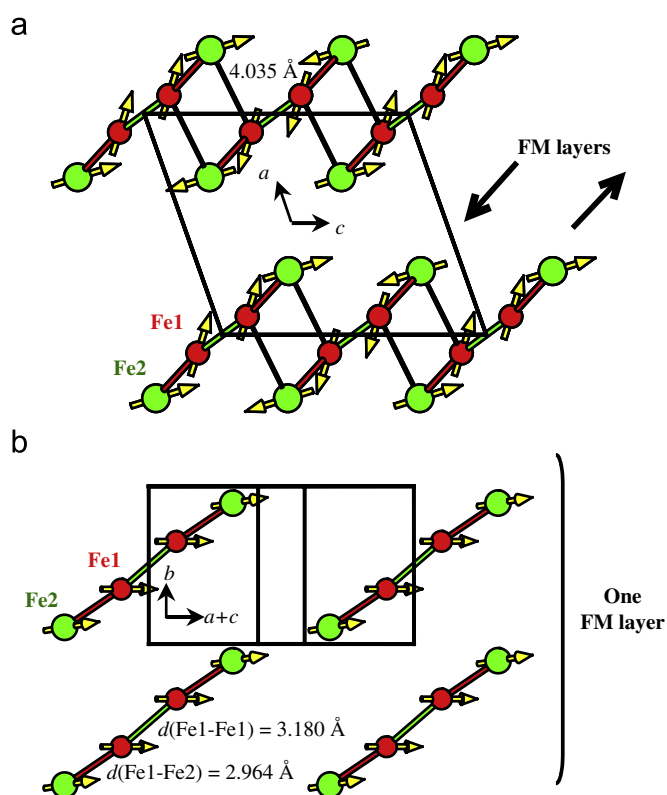


Fig. 2. Arrangements of four-spin cluster units (without oxygen atoms) in $\text{SrFe}_2(\text{PO}_4)_2$: (a) along the b -axis and (b) perpendicular to the $(a+c)$ direction. On panel b , the projection of only one layer is given. The arrows on the Fe atoms show the direction of magnetic moments at 3.5 K determined in this work. Bold lines show connections between Fe atoms in the four-spin cluster units (see Fig. 1). Connections between the four-spin cluster units (through long Fe2–O1 distances [28]) are shown by thin lines in panel a ($d(\text{Fe1}-\text{Fe2}) = 4.035 \text{ \AA}$).

transition because no anomalies were detected in the temperature dependence of magnetization curves. Below T_1 , weak ferromagnetic properties were found. $\text{SrFe}_2(\text{PO}_4)_2$ showed complex field-dependent magnetic susceptibilities and specific heat that

suggested a complex and interesting magnetic phase diagram [28]. Detailed investigations showed that there are at least five different magnetic phases of $\text{SrFe}_2(\text{PO}_4)_2$ as functions of temperature and magnetic field [29]. Note that physical properties of compounds containing Fe^{2+} ions, for example, FeCl_2 and FeBr_2 , have attracted much attention due to strong anisotropy and metamagnetic phase transitions [30–32]. The magnetic phase diagram of $\text{SrFe}_2(\text{PO}_4)_2$ seems to be as complex as those of FeCl_2 and FeBr_2 .

In this work we report on magnetic properties of $\text{SrFe}_2(\text{PO}_4)_2$ studied by neutron powder diffraction (NPD), ac and dc magnetization, and specific heat. Neutron diffraction clearly reveals the magnetic origin of the phase transitions at both T_1 and T_2 . The magnetic structure below T_1 at zero magnetic field was determined.

2. Experimental

Single-phase $\text{Sr}_3(\text{PO}_4)_2$ and FePO_4 were prepared from mixtures of SrCO_3 (99.99%), $\text{NH}_4\text{H}_2\text{PO}_4$ (99.999%), and Fe_2O_3 (99.9%), by the solid state method. The mixtures were contained in alumina crucibles, heated under air while increasing temperature very slowly from RT to 873 K, reground, and allowed to react at 1153 K for $\text{Sr}_3(\text{PO}_4)_2$ and 1053 K for FePO_4 for 120 h with four intermediate grindings. The $\text{SrFe}_2(\text{PO}_4)_2$ sample ($\sim 7.5 \text{ g}$) was synthesized by the solid state method from a stoichiometric mixture of the $\text{Sr}_3(\text{PO}_4)_2$ and FePO_4 materials and Fe (99.9%). The powder mixture was placed in a Pt crucible, which was located in an evacuated quartz tube, and annealed at 1173 K for 200 h with five intermediate grindings. The product was cooled in a furnace. It was a dense dark-brown pellet. The reground powder sample was white. The sample was single-phased according to X-ray powder diffraction.

Magnetic susceptibilities, $\chi = \mathbf{M}/\mathbf{H}$, of $\text{SrFe}_2(\text{PO}_4)_2$ were measured on a DC SQUID magnetometer (Quantum Design, MPMS XL) from 20 to 4 K in applied fields of 0.01 and 1 T. Frequency dependent ac susceptibility measurements at zero static magnetic field were performed with a Quantum Design MPMS instrument from 20 to 2 K at frequencies (f) of 0.5, 7, 110, and 500 Hz and an applied oscillating magnetic field (H_{ac}) of $5 \times 10^{-4} \text{ T}$. The ‘ac’ susceptibilities were also measured at $f = 110 \text{ Hz}$ using $H_{ac} = 10^{-6}$, 5×10^{-6} , and $2.5 \times 10^{-5} \text{ T}$; however, no dependence on H_{ac} was observed. Specific heat, $C_p(T)$, was recorded from 300 to 1.8 K in zero magnetic field by a pulse relaxation method using a commercial calorimeter (Quantum Design PPMS).

The NPD data for $\text{SrFe}_2(\text{PO}_4)_2$ were collected using the BT-1 high-resolution powder diffractometer at the NIST Center for Neutron Research, employing Cu (311) monochromator to produce a monochromatic neutron beam of wavelength 1.5403 Å. Collimators with horizontal divergences of 15', 20', and 7' full width at half maximum were used before and after the monochromator, and after the sample, respectively. The intensities were measured in steps of 0.05° in the 2θ range $3\text{--}168^\circ$. In order to study the magnetic structure and transitions, data were collected between 3.5 and 295 K. The structure analysis was performed using the program GSAS [33]. The neutron scattering amplitudes used in the refinements were 0.702, 0.945, 0.513, and $0.581 (\times 10^{-12} \text{ cm})$ for Sr, Fe, P, and O, respectively.

3. Results and discussion

Fig. 3 presents plots of magnetization (\mathbf{M}), χT , and $d(\chi T)/dT$ against temperature, T , for $\text{SrFe}_2(\text{PO}_4)_2$ measured at 0.01 and 1 T. Clear peaks, whose positions depended on the field, were seen

near T_1 . However, only a very small anomaly was detected on the $d(\chi T)/dT$ vs T curves at T_2 . The detection of this anomaly required the measurements with a fine step of 0.2 K. The ac susceptibility measurements showed no anomaly at T_2 , but sharp peaks for both χ' vs T and χ'' vs T curves at T_1 indicating the presence of a ferromagnetic contribution (Fig. 4). Specific heat measurements showed a weak, broad λ -type anomaly near T_2 and a sharp peak at T_1 . No other anomalies were found between 1.8 and 300 K (Fig. 5).

Fig. 6 shows a portion of the NPD patterns between 3.5 and 15 K. A few extra diffraction peaks were clearly observed between 8.5 and 10 K. The two strongest peaks could be indexed with a propagation vector $k = [0, \frac{1}{2}, \frac{1}{2}]$ referring to the crystal unit cell at 15 K. However, weak reflections marked by an oval in Fig. 6 showed small shifts from the expected positions. Below 7 K, new extra diffraction peaks with large intensities appeared, while those observed between 8.5 and 10 K disappeared. Below 7 K, the magnetic peaks can be indexed with a propagation vector $k = [0, 0, 0]$ referring to the unit cell at 15 K, indicating that the magnetic and crystal unit cells are the same.

Fig. 7 depicts the temperature dependence of the intensity of two representative magnetic peaks, $(-1\frac{11}{22})$ and (-101) . The $(-1\frac{11}{22})$ peak appeared below 11 K, reached its maximum intensity at 8.5 K, then gradually weakened, and disappeared below 7 K. The (-101) peak appeared below 7 K. Temperature hysteresis was observed near 7 K indicating that this phase transition is first order, while no hysteresis was found at 11 K, suggesting the phase transition of second order.

Structure parameters at RT [28] were used as the starting model for the structure refinement at 15 K. Table 1 lists lattice parameters, R factors, and the final refined positional and thermal parameters. Fig. 8a displays observed, calculated, and difference NPD patterns for $\text{SrFe}_2(\text{PO}_4)_2$ at 15 K. In the magnetically disordered phase above T_2 , correlations between magnetic moments of Fe give rise to a broad diffuse peak near $2\theta = 10^\circ$

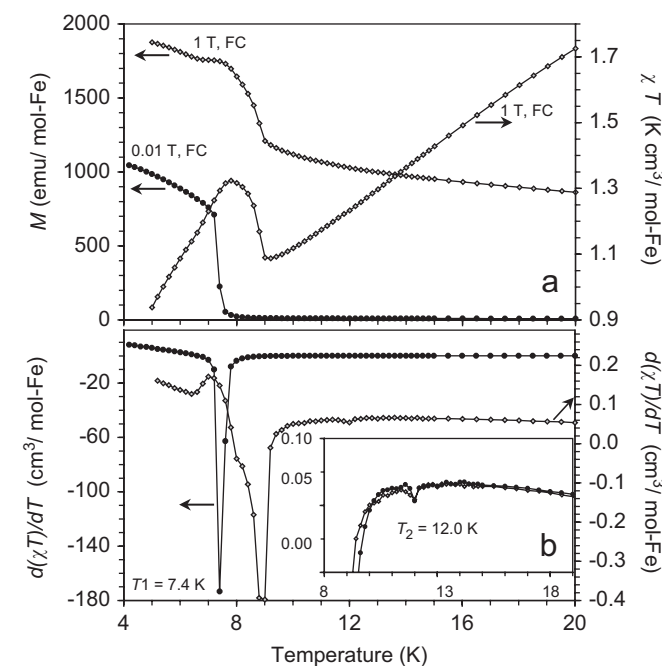


Fig. 3. (a) M vs T curves measured at 0.01 and 1 T (the left-hand axis) and the χT vs T curve measured at 1 T (the right-hand axis) from 20 to 4 K. (b) The $d(\chi T)/dT$ vs T curves at 0.01 T (the left-hand axis) and 1 T (the right-hand axis). The inset shows the region near $T_2 = 12$ K.

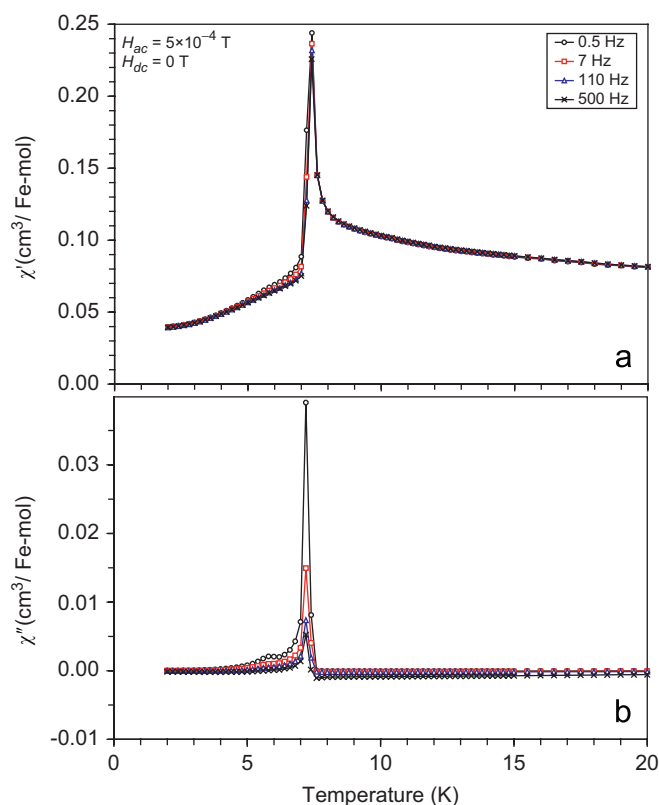


Fig. 4. (a) Real χ' and (b) imaginary χ'' parts of the ac susceptibility as a function of temperature (at 2–20 K) at frequencies $f = 0.5, 7, 110,$ and 500 Hz. Measurements were performed on cooling in zero static field using an ac field with the amplitude $H_{ac} = 5 \times 10^{-4}$ T.

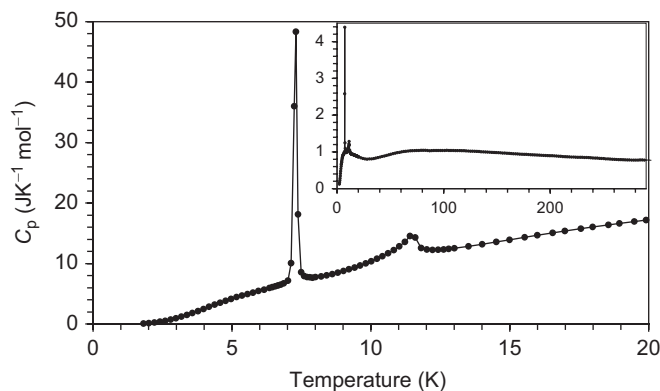


Fig. 5. C_p vs T curve between 1.8 and 20 K for $\text{SrFe}_2(\text{PO}_4)_2$. The inset shows the C_p/T ($\text{J K}^{-2} \text{mol}^{-1}$) vs T (K) curve between 1.8 and 300 K. Measurements were performed using a dense pellet in comparison with cold-pressed powder in [28]; as a result, the peak near 7.4 K is much more pronounced.

(Fig. 8a). This diffuse peak disappeared when the magnetic ordering is achieved.

Because only a few relatively weak magnetic reflections appear between 8.5 and 10 K (Fig. 6) and the magnetic unit cell is either relatively large or the magnetic structure is incommensurate, we were unable to determine the magnetic structure in this temperature range. The shifts of the weak reflections from the expected positions based on a simple commensurate magnetic structure suggest that incommensurate magnetic ordering may

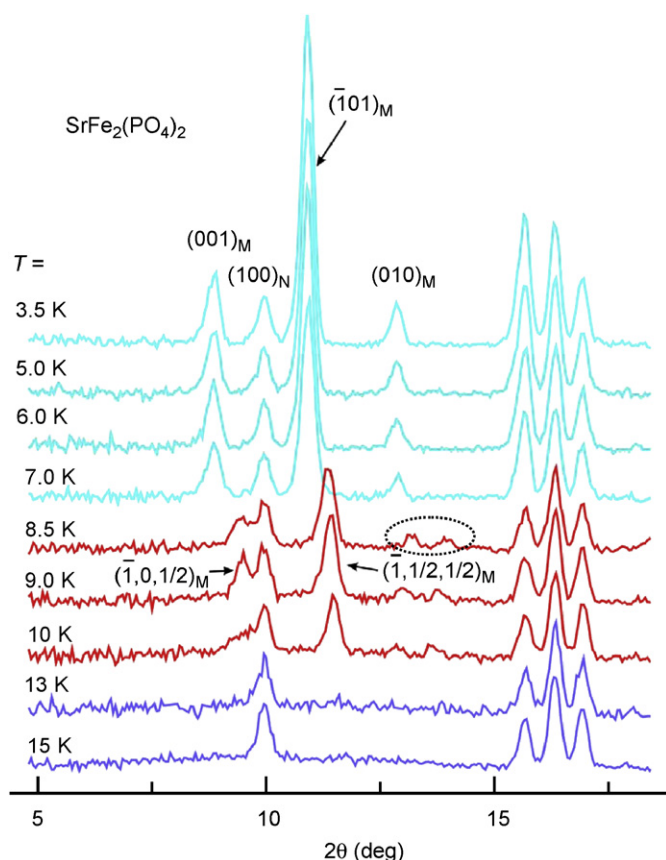


Fig. 6. Neutron powder diffraction patterns for $\text{SrFe}_2(\text{PO}_4)_2$ at different temperatures. Indices of some reflections are given, where M denotes magnetic reflections, and N denotes nuclear reflections.

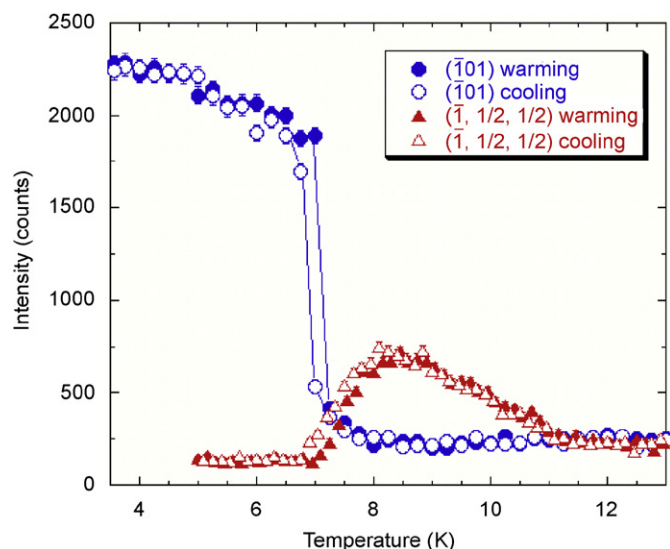


Fig. 7. Temperature dependence of the intensities of representative magnetic reflections (-101) and $(-1, \frac{1}{2}, \frac{1}{2})$ during cooling and heating.

take place. This suggestion is also supported by noticeable temperature shifts of the magnetic reflections between 8.5 and 10 K in comparison with undetectable temperature shifts of the magnetic reflections between 3.5 and 7 K. Because $k = [0,0,0]$ at 3.5 K, the magnetic structure was determined with the magnetic

Table 1

Fractional coordinates and isotropic atomic displacement parameters for $\text{SrFe}_2(\text{PO}_4)_2$ at 15 and 3.5 K^a

	x	y	z	10^2U (\AA^2)
Site^b				
Sr	0.3026(2)	0.1219(3)	0.0162(2)	0.23(4)
Fe1	0.0814(2)	0.6495(2)	0.1172(2)	0.20(3)
Fe2	0.2859(2)	0.8929(2)	0.3357(2)	0.25(3)
P1	0.0353(3)	0.1697(4)	0.1695(3)	0.45(6)
P2	0.4250(3)	0.8551(4)	0.6225(3)	0.43(5)
O1	0.1076(3)	0.2039(4)	0.3231(3)	0.33(6)
O2	0.1090(3)	-0.0150(4)	0.1373(3)	0.35(5)
O3	0.1373(3)	0.6538(4)	0.3579(2)	0.38(5)
O4	0.0653(3)	0.3405(4)	0.0842(2)	0.34(5)
O5	0.4264(3)	0.0848(4)	0.2725(3)	0.44(5)
O6	0.4483(3)	0.6843(4)	0.5378(3)	0.40(5)
O7	0.3471(3)	0.0169(4)	0.5222(3)	0.60(6)
O8	0.3089(3)	0.6945(3)	0.1952(2)	0.56(5)
Site^c				
Sr	0.30276(17)	0.1214(2)	0.01606(16)	0.33(3)
Fe1	0.08144(13)	0.64973(16)	0.11752(12)	0.23(3)
Fe2	0.28629(14)	0.89340(17)	0.33581(11)	0.26(2)
P1	0.0350(2)	0.1698(3)	0.1697(2)	0.45(5)
P2	0.4254(2)	0.8547(3)	0.6220(2)	0.34(4)
O1	0.1075(2)	0.2041(3)	0.3232(2)	0.48(4)
O2	0.1093(2)	-0.0155(3)	0.1373(2)	0.37(4)
O3	0.1371(2)	0.6544(3)	0.3577(2)	0.39(4)
O4	0.0657(2)	0.3412(3)	0.0847(2)	0.43(4)
O5	0.4263(2)	0.0839(3)	0.2724(2)	0.52(4)
O6	0.4481(2)	0.6840(3)	0.5376(2)	0.50(4)
O7	0.3477(2)	0.0165(3)	0.5223(2)	0.45(4)
O8	0.3087(2)	0.6948(3)	0.1955(2)	0.58(4)

The magnetic moment coordinates are in the orthogonal system with $x \parallel a$, $y \parallel b^*$, and $z \parallel a \times b^*$.

^a Space group $P2_1/c$ (No. 14, cell choice 1); $Z = 4$. The occupancies of all the sites are 1. The Wyckoff notation of all the sites is $4e$.

^b $T = 15$ K: $a = 9.35417(13)$ \AA , $b = 6.83808(10)$ \AA , $c = 10.51899(15)$ \AA , $\beta = 109.5147(7)^\circ$, and $V = 634.192(16)$ \AA^3 ; $R_{wp} = 0.0399$, $R_p = 0.0334$, and $\chi^2 = 1.04$.

^c $T = 3.5$ K: $a = 9.35527(9)$ \AA , $b = 6.83869(7)$ \AA , $c = 10.52014(10)$ \AA , $\beta = 109.5176(5)^\circ$, and $V = 634.381(10)$ \AA^3 ; $R_{wp} = 0.0309$, $R_p = 0.0250$, and $\chi^2 = 1.899$; $M_x = 3.38(4)$ μ_B , $M_y = -0.20(8)$ μ_B , $M_z = 2.29(5)$ μ_B , and $M = 4.09(3)$ μ_B for Fe1 and $M_x = -0.09(6)$ μ_B , $M_y = 0.93(9)$ μ_B , $M_z = 3.96(4)$ μ_B , and $M = 4.07(4)$ μ_B for Fe2.

symmetry and unit cell similar to the crystal symmetry $P2_1/c$ and crystal unit cell. The magnetic and crystal structures were refined assuming one phase. No change in the crystal structure was found at low temperatures. In initial models of the magnetic structure, we assumed collinear antiferromagnetic structures with the magnetic moments along the main crystallographic axes. All three initial models converged to the same final magnetic structure. The final lattice parameters, R factors, refined magnetic moments, positional and thermal parameters are given in Table 1, and selected bond lengths and angles in Table 2. Figs. 8b and 9 display observed, calculated, and difference NPD patterns for $\text{SrFe}_2(\text{PO}_4)_2$ at 3.5 K.

The representation of the magnetic structure of $\text{SrFe}_2(\text{PO}_4)_2$ below 7 K is shown in Figs. 1, 2, and 10. The magnetic moments of the inner Fe1–Fe1 atoms of the four-spin cluster unit are ferromagnetically coupled (Figs. 1 and 2). The sign of superexchange interactions is well understood for a cation–anion–cation pathway. For a linear 180° bond angle, the interaction is antiferromagnetic, and ferromagnetic for an angle of 90° . The crossover takes place near 100° . In $\text{SrFe}_2(\text{PO}_4)_2$, the Fe1–O4–Fe1 bond angles are 96.9° which suggests ferromagnetic coupling. The magnetic moment of the outer Fe2 atom is also ferromagnetically coupled with that of the Fe1 atom but with spin canting. The Fe1–O–Fe2 bond angles are 79.8° , 80.6° , and 92.6° . The four-spin

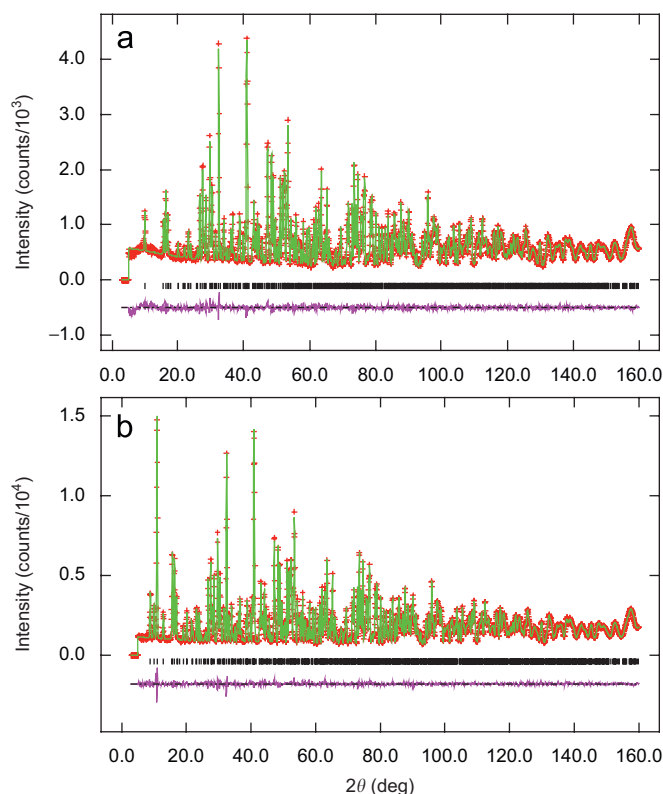


Fig. 8. The full observed (crosses), calculated (solid line), and difference NPD patterns for $\text{SrFe}_2(\text{PO}_4)_2$ at (a) 15 K and (b) 3.5 K.

Table 2

Bond lengths, l , and angles, ϕ , in $\text{SrFe}_2(\text{PO}_4)_2$ at 3.5 K

Bonds	l (Å)	Bonds	l (Å)
Sr1–O7	2.509(3)	Fe2–O1	2.680(2)
Sr1–O6	2.461(3)	Fe2–O2	2.276(2)
Sr1–O5	2.568(2)	Fe2–O3	2.211(2)
Sr1–O1	2.530(2)	Fe2–O5	2.107(2)
Sr1–O6'	2.611(3)	Fe2–O6	2.589(2)
Sr1–O3	2.648(3)	Fe2–O7	2.033(2)
Sr1–O2	2.706(2)	Fe2–O8	2.067(2)
Sr1–O4	2.961(3)	Fe2–O7'	3.304(2)
Sr1–O8	3.465(3)		
Fe1–O1	2.095(2)	P1–O1	1.546(3)
Fe1–O2	2.306(2)	P1–O2	1.536(3)
Fe1–O3	2.403(2)	P1–O3	1.541(3)
Fe1–O4	2.113(2)	P1–O4	1.558(3)
Fe1–O4'	2.135(2)	P2–O5	1.519(3)
Fe1–O8	2.031(2)	P2–O6	1.524(3)
Fe1–O7	3.189(2)	P2–O7	1.531(3)
Fe1–O3'	3.239(2)	P2–O8	1.570(3)
Angles	ϕ (deg)	Angles	ϕ (deg)
O1–P1–O2	106.48(16)	O5–P2–O6	111.48(17)
O1–P1–O3	105.75(15)	O5–P2–O7	114.22(17)
O1–P1–O4	112.58(17)	O5–P2–O8	108.38(15)
O2–P1–O3	115.08(16)	O6–P2–O7	106.32(16)
O2–P1–O4	108.03(16)	O6–P2–O8	112.11(17)
O3–P1–O4	109.00(16)	O7–P2–O8	104.17(15)
Fe1–O2–Fe2	80.59(8)		
Fe1–O3–Fe2	79.80(7)	Fe1–O4–Fe1	96.91(9)
Fe1–O8–Fe2	92.62(9)		

cluster units form ferromagnetic layers parallel to the $[-101]$ plane, and these layers are stacked antiferromagnetically in the $[-101]$ direction (Fig. 2). Spin canting of the outer atoms Fe2

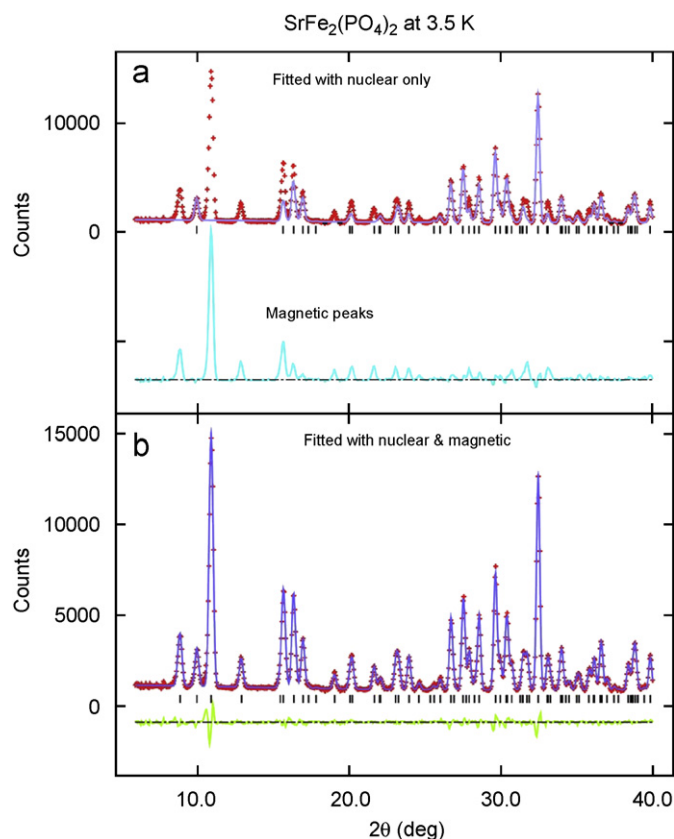


Fig. 9. (a) Portion of the observed (crosses), calculated (solid line), and difference NPD patterns for $\text{SrFe}_2(\text{PO}_4)_2$ at 3.5 K when only the nuclear structure was taken into account. Bragg reflections are indicated by tick marks. (b) Portion of the observed (crosses), calculated (solid line), and difference NPD patterns when the nuclear and magnetic structures were taken into account.

provides a weak ferromagnetic moment of about $1 \mu_B$ along the b -axis. The values obtained for the magnetic moments at 3.5 K are $4.09 \mu_B$ for Fe1 and $4.07 \mu_B$ for Fe2 in good agreement with the expected value of $4 \mu_B$ for Fe^{2+} . Fig. 11 shows the thermal evolution of the ordered magnetic moments between 3.5 and 7 K. The ferromagnetic component M_y of Fe2 decreases smoothly from $\sim 1 \mu_B$ to zero when the temperature increases from 5 to 7 K. The total ordered magnetic moment M of Fe1 is almost temperature independent, while M of Fe2 decreases from $4.07 \mu_B$ at 3.5 K to $2.7 \mu_B$ at 7 K. Magnetic moments of the *inner* Fe1–Fe1 atoms of the four-spin cluster units are coupled ferromagnetically and, therefore, seem to be very rigid. Magnetic moments of the *outer* Fe2 atoms are more flexible to temperature variations especially the canting angle.

Neutron diffraction unambiguously confirmed that the phase transition at T_2 has a magnetic origin, even though magnetization measurements were barely able to detect this phase transition. The negative gradient of the $d(\chi T)/dT$ vs T curve at T_2 suggests that a very weak ferromagnetic component should appear below T_2 . The weak magnetic reflections below T_2 indicate that the ordered moments of Fe are small compared with the full ordering of magnetic moments of Fe below T_1 , as expected at elevated temperatures.

In conclusion, the magnetic structure of $\text{SrFe}_2(\text{PO}_4)_2$ below $T_1 = 7.4$ K was determined. The spin canting provides a ferromagnetic component along the b -axis and explains the observed weak ferromagnetic properties. Neutron diffraction confirmed the magnetic origin of the phase transition at $T_2 = 11.4$ K.

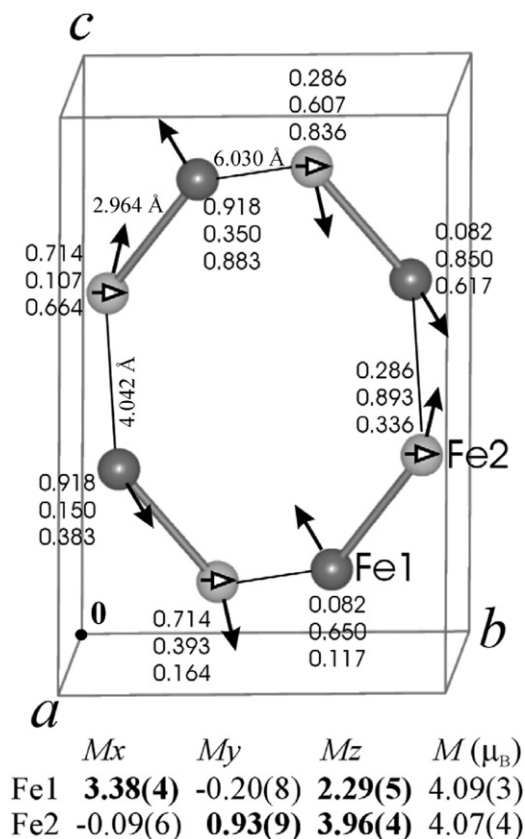


Fig. 10. The arrangement of Fe atoms in the structure of $\text{SrFe}_2(\text{PO}_4)_2$ in one unit cell. The coordinates for each Fe atoms in the unit cell are shown. The refined magnetic moments at 3.5 K are given at the bottom of the figure. The black arrows show the magnetic moment direction for each Fe ion, and the white arrows indicate the M_y component for the Fe2 ions which arrange ferromagnetically. Some Fe–Fe distances are given. Bold lines with $d(\text{Fe1–Fe2}) = 2.964 \text{ \AA}$ belong to the four-spin cluster units (see Figs. 1 and 2). The Fe1–Fe1 connections from the four-spin cluster units are not shown here because only one unit cell is given (see Fig. 2).

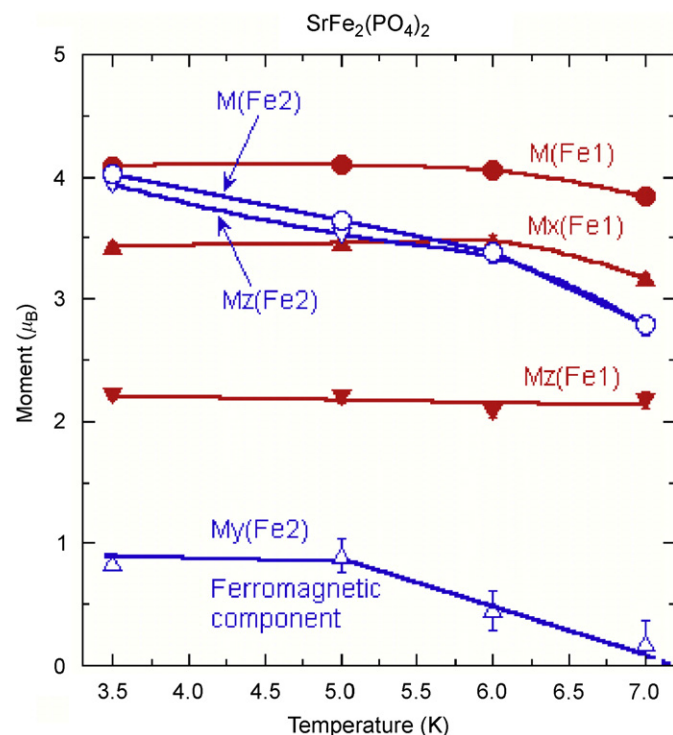


Fig. 11. Ordered magnetic moments of Fe ions in $\text{SrFe}_2(\text{PO}_4)_2$ as a function of temperature below 7 K. The ferromagnetic component M_y of Fe2 decreases smoothly from $\sim 1 \mu_B$ to zero when the temperature increases from 5 to 7 K.

Acknowledgements

This work was supported by World Premier International Research Center Initiative (WPI Initiative, MEXT, Japan).

References

- [1] S.-W. Cheong, M. Mostovoy, *Nature Mater.* 6 (2007) 13.
- [2] W. Eerenstein, N.D. Mathur, J.F. Scott, *Nature* 442 (2006) 759; D.I. Khomskii, *J. Magn. Magn. Mater.* 306 (2006) 1.
- [3] N.A. Hill, *J. Phys. Chem. B* 104 (2000) 6694.
- [4] K. Taniguchi, N. Abe, T. Takenobu, Y. Iwasa, T. Arima, *Phys. Rev. Lett.* 97 (2006) 097203; O. Heyer, N. Hollmann, I. Klassen, S. Jodlauk, L. Bohaty, P. Becker, J.A. Mydosh, T. Lorenz, D. Khomskii, *J. Phys.: Condens. Matter* 18 (2006) L471.
- [5] S. Park, Y.J. Choi, C.L. Zhang, S.-W. Cheong, *Phys. Rev. Lett.* 98 (2007) 057601.
- [6] Y. Naito, K. Sato, Y. Yasui, Y. Kobayashi, Y. Kobayashi, M. Sato, *J. Phys. Soc. Japan* 76 (2007) 023708.
- [7] G. Lawes, A.B. Harris, T. Kimura, N. Rogado, R.J. Cava, A. Aharony, O. Entin-Wohlman, T. Yildirim, M. Kenzelmann, C. Broholm, A.P. Ramirez, *Phys. Rev. Lett.* 95 (2005) 087205.
- [8] S. Jodlauk, P. Becker, J.A. Mydosh, D.I. Khomskii, T. Lorenz, S.V. Streltsov, D.C. Hezel, L. Bohaty, *J. Phys.: Condens. Matter* 19 (2007) 432201.
- [9] P.D. Battle, T.C. Gibb, G. Hu, D.C. Munro, J.P. Attfield, *J. Solid State Chem.* 65 (1986) 343.
- [10] J.P. Attfield, P.D. Battle, A.K. Cheetham, *J. Solid State Chem.* 57 (1985) 357.
- [11] J. Escobal, J.L. Pizarro, J.L. Mesa, J.M. Rojo, B. Bazan, M.I. Arriortua, T. Rojo, *J. Solid State Chem.* 178 (2005) 2626.
- [12] J. Escobal, J.L. Pizarro, J.L. Mesa, A. Larranaga, J.R. Fernandez, M.I. Arriortua, T. Rojo, *J. Solid State Chem.* 179 (2006) 3052.
- [13] I. de Pedro, J.M. Rojo, J.L. Pizarro, J.R. Fernandez, J.S. Marcos, M. Teresa Fernandez-Diaz, M. Arriortua, T. Rojo, *J. Mater. Chem.* 17 (2007) 3915.
- [14] K. Maass, R. Glaum, R. Gruehn, *Z. Anorg. Allg. Chem.* 628 (2002) 1663.
- [15] B. Elbali, A. Boukhari, R. Glaum, M. Gerk, K. Maass, *Z. Anorg. Allg. Chem.* 626 (2000) 2557.
- [16] B. Elbali, A. Boukhari, E.M. Holt, J. Aride, *J. Crystallogr. Spectrosc. Res.* 23 (1993) 1001.
- [17] B. Elbali, A. Boukhari, J. Aride, F. Abraham, *J. Solid State Chem.* 104 (1993) 453.
- [18] A. Hemon, G. Courbion, *J. Solid State Chem.* 85 (1990) 164.
- [19] Z. Bircsak, W.T. Harrison, *Acta Crystallogr. Sect. C* 54 (1998) 1554.
- [20] A. Moqine, A. Boukhari, J. Darriet, *J. Solid State Chem.* 107 (1993) 362.
- [21] J.F. Sarver, M.V. Hoffman, F.A. Hummel, *J. Electrochem. Soc.* 108 (1961) 1103.
- [22] J.R. Looney, J.J. Brown, *J. Electrochem. Soc.* 118 (1971) 470.
- [23] N. Faza, W. Treutmann, D. Babel, *Z. Anorg. Allg. Chem.* 627 (2001) 687; P. Gaveau, J.P. Boucher, L.P. Regnault, Y. Henry, *J. Appl. Phys.* 69 (1991) 6228; L.P. Regnault, J.Y. Henry, J. Rossat-Mignod, A. De Combarieu, *J. Magn. Magn. Mater.* 15–18 (1980) 1021.
- [24] A.A. Belik, M. Azuma, A. Matsuo, M.H. Whangbo, H.J. Koo, J. Kikuchi, T. Kaji, S. Okubo, H. Ohta, K. Kindo, M. Takano, *Inorg. Chem.* 44 (2005) 6632.
- [25] A.A. Belik, M. Azuma, A. Matsuo, T. Kaji, S. Okubo, H. Ohta, K. Kindo, M. Takano, *Phys. Rev. B* 73 (2006) 024429.
- [26] H.J. Koo, M.H. Kang, *Solid State Sci.* 9 (2007) 955.
- [27] A.A. Belik, B.I. Lazoryak, K.V. Pokholok, T.P. Terekhina, I.A. Leonidov, E.B. Mitberg, V.V. Karelina, D.G. Kellerman, *J. Solid State Chem.* 162 (2001) 113.
- [28] A.A. Belik, M. Azuma, M. Takano, B.I. Lazoryak, *Chem. Mater.* 16 (2004) 4311.
- [29] A.A. Belik, E. Takayama-Muromachi, in preparation.
- [30] R.J. Birgeneau, G. Shirane, M. Blume, W.C. Koehler, *Phys. Rev. Lett.* 33 (1974) 1098.
- [31] H. Aruga Katori, K. Katsumata, M. Katori, *Phys. Rev. B* 54 (1996) 9620(R).
- [32] H. Aruga Katori, K. Katsumata, O. Petravic, W. Kleemann, T. Kato, *Ch. Binck, Phys. Rev. B* 63 (2001) 132408.
- [33] A. Larson, R.B. Von Dreele, Los Alamos National Laboratory, Internal Report, 1994.